

Theoretical design of superhard twinned BC₂N

Nan Min ^{a,b}, Hui Liang ^a, Hao Chen ^c, Xianqi Song ^{a,*}, Dan Zhou ^{c,**}, Quan Li ^{a,b,*}

^a State Key Lab of Superhard Materials and Key Laboratory of Material Simulation Methods & Software of Ministry of Education, College of Physics, Jilin University, Changchun 130012, China

^b International Center of Future Science, Jilin University, Changchun 130012, China

^c School of Physics, Changchun University of Science and Technology, Changchun 130022, China

ARTICLE INFO

Keywords:

Twin boundary
First principles
Superhard materials
BC₂N

ABSTRACT

BC₂N is an ideal combination of diamond and boron nitride and is expected to exhibit better mechanical properties and thermal stability than boron nitride and diamond, respectively. Recent studies raise exciting prospects of building coherent nanotwinned boundaries to improve performance of ceramics. Herein, we developed a systematic method to construct twin structures of BC₂N. The newly identified nanotwinned BC₂N variant (τ -BC₂N) exhibits better energetic stability and higher mechanical strength than single-crystal BC₂N, attributed to the optimized bonding behavior and crystal orientations induced via twinning. The simulated X-ray diffraction patterns of τ -BC₂N match those reported in previous experimental data. The nanotwinned BC₂N displays superior Vickers hardness of ~140 GPa, surpassing that of diamond. The computationally tailored approach and results obtained by twin-strengthening strategies offer powerful insights for the rational design and functional optimization of nanotwinned boron–carbon–nitrogen compounds containing intricate multiautomatic constituents and structures.

Superhard materials with Vickers hardness (H_V) exceeding 40 GPa are widely used in industrial applications, such as device processing, fine grinding, and geological exploration [1–3]. Single-crystal cubic diamond is a typical superhard material with ultrahigh hardness (62–110 GPa) [4]. However, it exhibits poor thermal stability and chemical inertness for cutting ferrous metals. Cubic boron nitride (*c*-BN), a traditional superhard material, exhibits better thermal and chemical stability than diamond; however, its H_V remains limited at 45–63 GPa [5,6]. The similarities between the covalent bond networks and excellent mechanical properties of diamond and *c*-BN have spurred interest in superhard boron–carbon–nitrogen (B–C–N) materials with all-*sp*³ strong covalent bonds [7–14]. Such materials are expected to possess dual advantages of improved mechanical properties and chemical inertness. Extensive efforts have been invested in synthesizing and characterizing diverse B–C–N compounds [15–21]. Most intriguing among them is *c*-BC₂N synthesized under high-temperature and -pressure with an experimental H_V of 62–76 GPa [20,21], surpassing that of *c*-BN. However, determining the crystal structures of BC₂N from the experimental X-ray diffraction (XRD) spectra is challenging because of the similarity and low atomic mass of B, C, and N. Employing advanced structural

design methods for superhard materials, theoretical researchers have successfully explored various BC₂N candidate structures. Rich structural diversities of BC₂N have been proposed, such as zinc-blende stru-*m* (*m* = 1–7), [22] tetragonal *z*-BC₂N [23], body-centered (*bc*6) BC₂N [24], wurtzite BC₂N [25], *R*3*m*-2 *u* BC₂N [26], and *dia*-BC₂N [15], offering abundant possibilities for optimizing the mechanical properties of BC₂N [16,27–30].

Grain-boundary engineering has been proven to be an effective approach for tailoring the mechanical properties of materials [31,32]. Recent studies have emphasized the importance of high-density coherent nanotwinned (*nt*) boundaries in enhancing the stability and mechanical properties of ceramics [4,33–37] owing to the unique low-energy and lattice-matched features of *nt*-boundaries compared with those of common grain boundaries. Surprisingly, *nt*-diamond and *nt*-BN exhibit a remarkable hardness of ~200 and 108 GPa, surpassing that of diamond and *c*-BN, respectively [4,33]. Simulated stress responses of *nt*-diamond and *nt*-BN reveal the underlying stiffening mechanism, indicating that *nt*-boundaries promote a strong stress concentration and drive bond realignment processes [38,39]. The expectation is to apply these strengthening effects to improve

* Corresponding authors at: State Key Lab of Superhard Materials and Key Laboratory of Material Simulation Methods & Software of Ministry of Education, College of Physics, Jilin University, Changchun 130012, China.

** Corresponding author at: School of Physics, Changchun University of Science and Technology, Changchun 130022, China.

E-mail addresses: sxq@calypso.cn (X. Song), zhoudan@cust.edu.cn (D. Zhou), liquan777@jlu.edu.cn (Q. Li).

performance of BC₂N and other ternary B–C–N materials. However, theoretically complex and experimentally indistinguishable bonding networks in these compounds immensely hinder the structure design and performance evaluation of *nt*-ternary B–C–N compounds.

Herein, we developed a systematic approach for designing twin structures and applied it to construct twinned BC₂N structures. Multiple twinned BC₂N structures with distinct bonding topologies were identified. Results revealed that increasing the ratio of C–C and B–N bonds in the twinned BC₂N structure increases its energetic stability. The developed twinned BC₂N structure, named τ -BC₂N, exhibited lower energy than its single-crystal β -BC₂N counterpart, and its simulated XRD patterns well matched those reported in the experimental data [20,21]. τ -BC₂N exhibited stepwise strengthening in stress responses and higher ideal pure/Vickers shear strength than monocrystal β -BC₂N. The theoretical hardness of *nt*-BC₂N reached \sim 140 GPa, exceeding that of diamond, owing to the size-dependent hardening effects in *nt*-BC₂N. These results reveal the twinned structures and twin-strengthening mechanism in BC₂N and provide an effective approach for the rational design and functional optimization of *nt*-B–C–N compounds.

All first-principles calculations were performed using the density functional theory (DFT) [40] with the Vienna ab initio simulation package code [43] using the local density approximation pseudopotential [41,42]. The projector-augmented wave (PAW) [44] described the electron-ion interaction with $2s^22p^1$, $2s^22p^2$, and $2s^22p^3$ for B, C, and N, respectively. Total-energy calculations employed a plane-wave kinetic energy cutoff of 700 eV and an $8 \times 8 \times 8$ k-mesh grid for the single crystal ($6 \times 6 \times 6$ for twinned crystals) according to the Monkhorst–Pack method [45]. The energy convergence, residual stresses, and forces in fully relaxed structures were maintained at <1 meV/atom, 0.1 GPa, and 0.001 eV/ \AA , respectively. Phonon calculations were performed using the direct supercell method implemented in the Phonopy code [46,47], with forces obtained via the Hellmann–Feynman theorem, for a simulated cell containing $2 \times 2 \times 2$ unit cells with a total of 384 atoms for τ -BC₂N. Elastic constants were determined using the efficient strain–stress method, and the elastic moduli were derived using the Voigt–Reuss–Hill method [48]. The H_V of covalent crystals was estimated using Tian’s revised Chen’s hardness model [49,50]. Relaxed loading paths and ideal strengths were determined using an established method [51–57], simultaneously relaxing atomic basis vectors and all the strain components orthogonal to applied stress at each step. The atomic positions, cell shape, and stress–strain relations were determined at each quasi-static step with a strain of 0.01 through the corresponding relaxation process.

We reported an effective methodology for designing superhard twin structures; the approach is outlined as follows. (i) Twin plane (TP) and matrix selection: TP serves as the interface between the matrix and twin parts. These two parts satisfy the mirror symmetry in relation to the TP. The matrix part, adaptable in thickness, is constructed from a slab model derived from sliced single crystals along the appropriate single-crystal plane. For structures containing complex units, different cutting positions of the crystal plane with the same Miller index produce different matrix parts. Ensuring a reasonable matrix and twin-part structure demands cutting in a sound position, aligning the TP with the mirror plane of the structural unit or avoiding cutting structural units of a single crystal to secure the bond matching on both sides of the TP. (ii) Interface bonding alignment: While TP selection reflects lattice orientation on both sides, interface bonding information is not determined. Introducing moderate translation at a fractional lattice vector or rotation at a specific angle (possibly with rotational symmetry relative to the normal axis of TP) in the twin part does not change the crystal orientation relationship on both sides of TP but can reduce structural volume, optimize bonding distribution, and reduce the interface energy. Therefore, the diversity of coherent twin structures is ensured by regulating crystal plane orientation, twin thickness, surface structure of the matrix part, and relative displacement (translation and rotation) between the matrix and twin parts. These operations are essential for optimal bonding matching and minimizing twin interface energy. All bonds, except for new bonding

modes near the TP, depend on single-crystal structures, greatly improving the search efficiency and rationality of twin structures during structural design.

β -BC₂N possessing the most stable zinc-blende structure with an eight-atom cell exhibits various bond types, including C–C, B–N, B–C, and C–N bonds. The atomic arrangement of β -BC₂N is similar to those of diamond and *c*-BN; however, diamond and *c*-BN contain single-type chemical bonds. The matrix parts of twinned BC₂N are obtained by cleaving β -BC₂N along the nonequivalent (111) and $(\bar{1}\bar{1}1)$ planes [Fig. 1(a)], and twin parts are available from rotation, translation, and mirror operations on matrix parts. After binding the matrix and twin parts, diverse twinned BC₂N structures are constructed. Structures are grouped in Fig. 1 according to the matrix-part and twin-part orientation, in which the combining types between matrix and twin parts are changed through relative translation and rotation to construct diverse structures. With twinning interface formation, newly introduced C–C, B–N, B–C, C–N, B–B, or N–N bonds may change bond ratios in BC₂N compounds and cause energy variation, surpassing the influence of twin thickness (λ) on energy variation. To estimate this impact, we identified 18 thinnest periodic coherent twin structures with distinct bonding topologies [Fig. 1(c)–(h)] and analyzed the relation between energy and bond ratio [Fig. 1(b)]. All these twinned structures contain C–C, B–N, B–C, and C–N bonds. Energy distribution based on B–B or N–N bond proportions is indicated by red, blue, and green regions shown in Fig. 1(b). Green squares, blue circles, and red triangles signify structures with 0.0 %, 2.1 %, and 4.2 % less stable bonds (B–B or N–N bonds), respectively. Notably, twinned BC₂N structures with higher proportions of B–B and N–N bonds disfavor and those with higher proportions of C–C and B–N bonds favor energy variation. Additional BC₂N twin-structure information is shown in Table S1 [58].

Notably, twinned BC₂N-1, named τ -BC₂N (Table S2) [58] with *Pmn2*₁ space group, contains \sim 58.3 % C–C and B–N bonds, exceeding β -BC₂N. The energy of τ -BC₂N is 75.4 meV/atom lower than β -BC₂N, affirming dynamic stability through the absence of imaginary frequencies in the phonon spectra (Fig. S1) [58]. Simulated XRD patterns for τ -BC₂N and previously proposed β -BC₂N were conducted using two experimental X-ray wavelengths: 0.4246 [20] [Fig. 2(a)] and 0.3738 \AA [21] [Fig. 2(b)]. Both structures align well with experimental main XRD peak positions and relative intensities. τ -BC₂N reproduces the experimental XRD peak observed at 21.0° as shown in [Fig. 2(a)]. The main peak broadening may stem from the contribution of peaks located at \sim 11.4° and \sim 12.7° of τ -BC₂N and the presence of amorphous grain boundary regions between nanocrystallites [20]. A similar phenomenon also appears in the other experimental data [21], where the main peak is much sharper, as shown in [Fig. 2(b)]. Here, we further present a combined theoretical spectrum for the phases of τ -BC₂N and β -BC₂N. The relative intensity of the experimental XRD peaks can be better explained by the combined contributions from the coexisting phases. The main peaks contributed by both of two phases appear more sharper, and the relative intensity of the experimental peaks could be modulated by the relative weight of the individual phases, indicating the possible coexistence of varying phases [15,22,23,26] and proportion in previous synthesized samples [20,21].

The calculated electronic properties of τ -BC₂N and β -BC₂N manifest that increased percentages of C–C and B–N bonds elevate the electronic band gap. In the context of a microscopic harness model, breaking an electron-pair bond in a crystal leads to two electrons transitioning from valence to conduction bands, correlating activation energy required for plastic glide to twice the electronic band gap, E_g [8]. Therefore, a higher electron density and E_g of τ -BC₂N implies its higher hardness compared to β -BC₂N [Fig. 3]. Simulated bulk (*B*), shear (*G*), and Young’s modulus of β -BC₂N is 410, 451, 990 GPa, respectively, are slightly lower than the corresponding elastic modulus of τ -BC₂N (415, 462, and 1012 GPa, respectively). This trend underscores the increased elasticity of τ -BC₂N owing to C–C and B–N bond ratios compared to β -BC₂N. The simulated

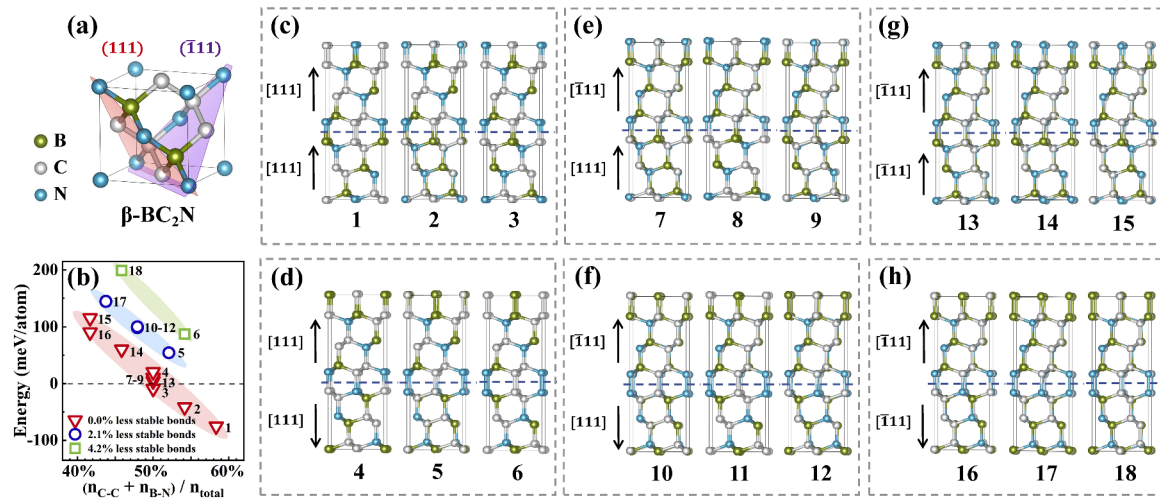


Fig. 1. (a) Crystal structures and cutting planes of β - BC_2N . (b) Energy change with the ratio of C-C and B-N bonds in the 18 constructed twin-like BC_2N structures relative to β - BC_2N values. Different stable bond ratios are represented by green squares (0.0 %), blue circles (2.1 %), and red triangles (4.2 %). (c)–(h) Twinned BC_2N structures of divided into six groups by gray dashed frames, according to the orientation of the matrix and twin part.

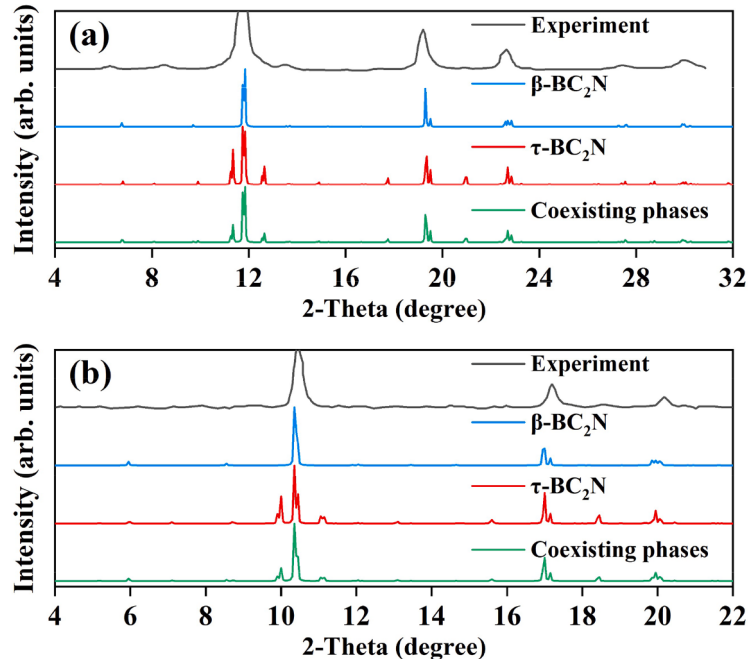


Fig. 2. Simulated X-ray diffraction for β - BC_2N , τ - BC_2N , and the above two coexisting phases with an average of the data from individual phases at a wavelength of (a) 0.4246 and (b) 0.3738 Å, compared with experimental results [20,21], respectively.

harness using the elastic model [49,50] stands at 80 GPa for τ - BC_2N , $H_V = 0.92 \cdot (G/B)^{1.137} \cdot G^{0.708}$, higher than β - BC_2N (78 GPa).

τ - BC_2N has been effectively utilized as an ideal periodic densest coherent twin model to clarify the twin-boundary (TB) effect on mechanical properties and relevant mechanisms in BC_2N . The actual productions of nano- BC_2N are usually polycrystalline covalent materials and the nt -boundaries maybe formed within each nanograin. The dual hardening effects, closely related to grain size (D) or λ , demand consideration. The hardness of nt - BC_2N can be evaluated using model [2] $H_V = H_0 + K_{\text{HP}} D^{-1/2} + K_{\text{qc}} D^{-1}$, where the hardness of a perfect single-crystal β - BC_2N (H_0) is 78 GPa [8]. The material-dependent Hall-Petch hardening coefficient K_{HP} [59,60] is set as 145 GPa·nm^{1/2}, an average between diamond (164 GPa·nm^{1/2}) and c -BN (126 GPa·nm^{1/2}) [4]. The theoretical quantum confinement hardening coefficient (K_{qc}) [61] for β - BC_2N is 162 GPa·nm ($K_{\text{qc}} = 211 N_e^{1/3} e^{-1.19 f_i}$ [50]),

where N_e is the number valence electrons per cubic angstroms [8], and f_i is the ionicity of chemical bonds in the crystal scaled by Phillips [62]. Combining these factors, the contribution from the two size effects on the hardness of nano- BC_2N is 62 GPa at the D (or λ) = 10 nm. Combined with the intrinsic hardness of single-crystal BC_2N , the H_V of nt - BC_2N reaches 140 GPa, surpassing that of diamond.

To evaluate the potential strengthening effect of TBs in nt - BC_2N , it is instructive to examine the stress-strain relations of τ - BC_2N along various directions under pure/Vickers shear loading conditions, comparing them with those of β - BC_2N . For β - BC_2N , the pure shear strength is 31.6 GPa at a strain of 0.08 along (110)[001] [Fig. S2(a)] [58], while the Vickers shear strength is 49.0 GPa at a strain of 0.09 along (001)[110] [Fig. S2(b)] [58]. τ - BC_2N exhibits the lowest pure shear peak of 43.4 GPa at a strain of 0.12 along (010)[001] direction [Fig. 4(a)] and the lowest Vickers shear peak value of 50.6 GPa at a strain of 0.13 along (001)[120]

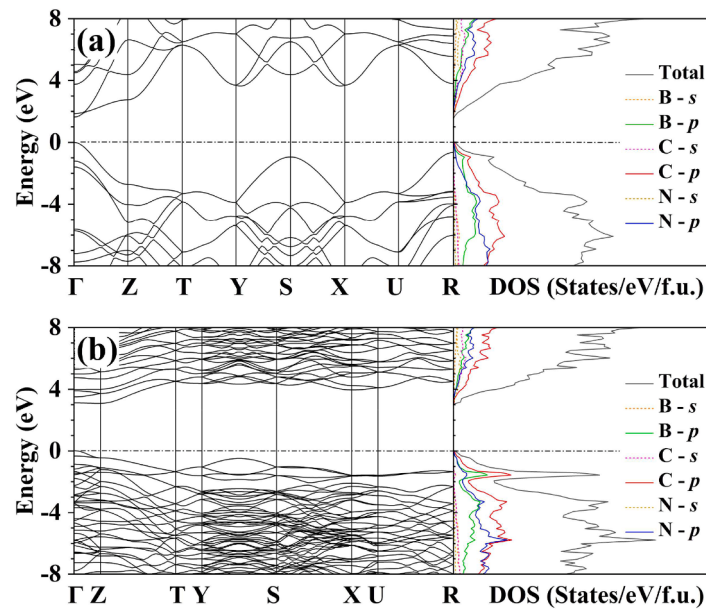


Fig. 3. Electronic band structures and density of states (DOS) of (a) $\beta\text{-BC}_2\text{N}$ and (b) $\tau\text{-BC}_2\text{N}$.

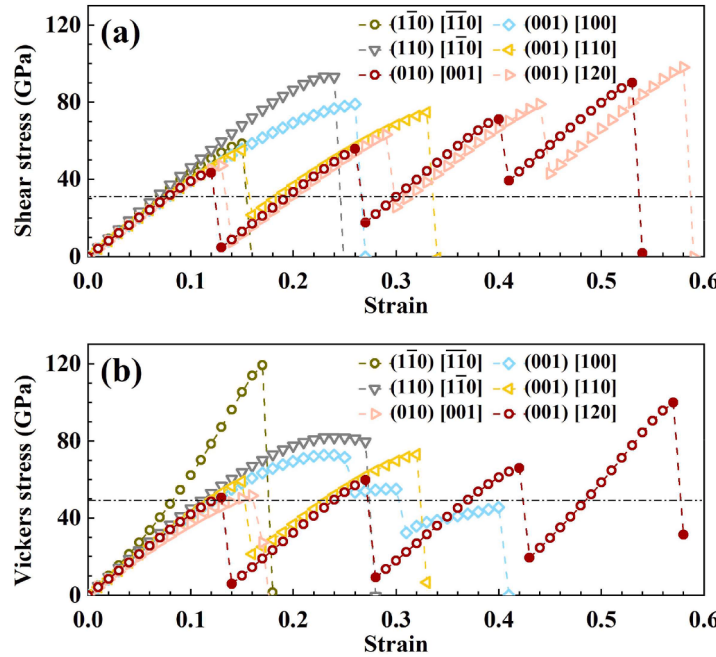


Fig. 4. (a) Pure shear stress–strain relations of $\tau\text{-BC}_2\text{N}$ along various shear directions. (b) Shear stress–strain relations of $\tau\text{-BC}_2\text{N}$ along various directions under Vickers indentation. Solid red points indicate peak stresses along the weakest shear direction, and dash-dotted lines mark the ideal pure/Vickers shear strength of $\beta\text{-BC}_2\text{N}$.

direction [Fig. 4(b)]. Interestingly, both pure and Vickers shear stress responses of $\tau\text{-BC}_2\text{N}$ along these “weakest” directions show continuous multistage reinforcements as saw-tooth patterns. This unique behavior stands in contrast to other known twinned structures like zinc-blende diamond [38], Si [63], BN [39], GaAs [64], and InSb [65].

To delve into the underlying mechanism of these distinct continuous multistage reinforcements, we visualize the evolution of key bond lengths within $\tau\text{-BC}_2\text{N}$ as the strain increases, capturing pivotal structural snapshots under pure shear (Fig. 5) and Vickers shear (Fig. S3) loading conditions. Remarkably, three instances of shear-stress releases and subsequent bond-rearrangement processes are observed along (010)[001] shear direction [Fig. 5(a)]. Initially, as strain increases, elongated

N-C₂ and B-C₁ bonds, along with shortened B-N and C₁-C₂ bonds in layer I, continuously resist shear deformation up to the strain of 0.12. Subsequently, a breaking of all bonds within layer I triggers an interlayer slip [Fig. 5(b)], resembling glide-set dislocations seen in *nt*-diamond [66,67]. At a strain of 0.13, the bond-rearrangement process in $\tau\text{-BC}_2\text{N}$ eliminates previous weak bonds within layer I, bolstering shear resistance and leading to a second-stage stress escalation, as shown in Fig. 4(a). This is followed by analogous slips appearing at strains of 0.26 to 0.27 within layer II and strains of 0.40 to 0.41 within layer III [Fig. 5(c) and 5(d)], respectively. These slips result in the peak stress increase from 43.4 GPa at the strain of 0.12 to 90.0 GPa at the strain of 0.53 in the (010)[001] direction and make this direction no longer be the weakest

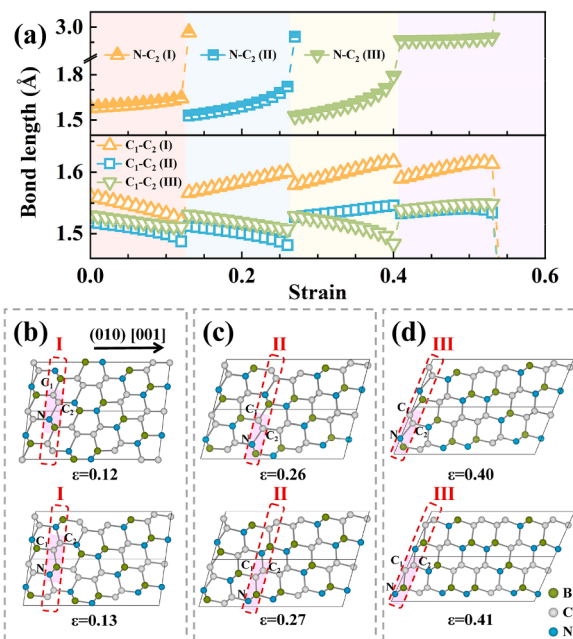


Fig. 5. (a) Variation of the key bond lengths in twinned BC₂N with increasing strain along (010)[001] direction under pure shear condition. (b)–(d) Structural snapshots of twinned BC₂N in three bond-rearrangement processes: layer I at the strain of 0.12, layer II at 0.26, and layer III at 0.40.

direction. The similar strengthening also occurs in the (001)[110] and (001)[120] directions. The shear strengthening causes the change in weakest direction from (010)[001] to (110)[110] with a peak stress of 58.6 GPa at the strain of 0.15. These results manifest the significant advantages in improving the shear strength and toughness within BC₂N by introducing TBs.

In summary, we systematically develop an effective approach to construct superhard twinned structures, benchmarked using ternary BC₂N materials with diverse bond types. The designed twinned structure τ -BC₂N possesses superior energetic stability and ideal strength compared to single-crystal β -BC₂N. The intricate interplay of crystal orientation optimization, stable covalent bond proportion, and size effects through TBs substantially contributes to improved energetic and mechanical properties. The simulated H_V of *nt*-BC₂N reaches 140 GPa, exceeding that of a single-crystal diamond. Under loading conditions, τ -BC₂N exhibits stepwise strengthening stress responses, accompanied by interlayer slips and bond flips parallel to the TPs, revealing reinforced mechanisms in *nt*-BC₂N. These insights raise prospects for advancing rational design and uncovering novel superhard twinned materials with light-element covalent compounds.

Declaration of Competing Interest

The authors declare that they have no known competing financial interests or personal relationships that could have appeared to influence the work reported in this paper.

Acknowledgments

This research is supported by the National Key Research and Development Program of China (Grant Nos. 2018YFA0703404 and 2021YFA1400503), Natural Science Foundation of China (Grant Nos. T2325013, 52288102, 12074140, and 11704044), China Postdoctoral Science Foundation (Grant No. 2023M731296), and Program for Jilin University Science and Technology Innovative Research Team. Reported calculations utilized computing facilities at the High-Performance Computing Center of Jilin University.

Supplementary materials

Supplementary material associated with this article can be found, in the online version, at doi:10.1016/j.scriptamat.2023.115843.

References

- [1] J. Haines, J.M. Leger, G. Bocquillon, Synthesis and design of superhard materials, *Annu. Rev. Mater. Res.* 31 (2001) 1–23.
- [2] Z.S. Zhao, B. Xu, Y.J. Tian, Recent advances in superhard materials, *Annu. Rev. Mater. Res.* 46 (2016) 383–406.
- [3] M.T. Yeung, R. Mohammadi, R.B. Kaner, Ultraincompressible, superhard materials, *Annu. Rev. Mater. Res.* 46 (2016) 465–485.
- [4] Q. Huang, D.L. Yu, B. Xu, W.T. Hu, Y.M. Ma, Y.B. Wang, Z.S. Zhao, B. Wen, J.L. He, Z.Y. Liu, Y.J. Tian, Nanotwinned diamond with unprecedented hardness and stability, *Nature* 510 (2014) 250–253.
- [5] N.V. Novikov, V.Y. Sirota, V.I. Mal'nev, I.A. Petrusha, Mechanical properties of diamond and cubic BN at different temperatures and deformation rates, *Diam. Relat. Mater.* 2 (1993) 1253–1256.
- [6] R.A. Andrievski, Superhard materials based on nanostructured high-melting point compounds: achievements and perspectives, *Int. J. Refract. Met. Hard Mater.* 19 (2001) 447–452.
- [7] D.M. Teter, R.J. Hemley, Low-compressibility carbon nitrides, *Science* 271 (1996) 53–55.
- [8] F.M. Gao, J.L. He, E.D. Wu, S.M. Liu, D.L. Yu, D.C. Li, S.Y. Zhang, Y.J. Tian, Hardness of covalent crystals, *Phys. Rev. Lett.* 91 (2003), 015502.
- [9] V.L. Solozhenko, O.O. Kurakevych, D. Andrault, Y.L. Godec, M. Mezouar, Ultimate metastable solubility of boron in diamond: synthesis of superhard diamondlike BC₅, *Phys. Rev. Lett.* 102 (2009), 015506.
- [10] M. Zhang, H.Y. Liu, Q. Li, B. Gao, Y.C. Wang, H.D. Li, C.F. Chen, Y.M. Ma, Superhard BC₃ in cubic diamond structure, *Phys. Rev. Lett.* 114 (2015), 015502.
- [11] X.Q. Song, C. Liu, Q. Li, Y.M. Ma, C.F. Chen, Intrinsic dense twinning via release of native strain, *Acta Mater.* 257 (2023), 119151.
- [12] S.S. Zhang, J.L. He, Z.S. Zhao, D.L. Yu, Y.J. Tian, Discovery of superhard materials via CALYPSO methodology, *Chin. Phys. B* 28 (2019), 106104.
- [13] W.C. Chen, J.N. Schmidt, D. Yan, Y.K. Vohra, C.C. Chen, Machine learning and evolutionary prediction of superhard B-C-N compounds, *npj, Comput. Mater.* 7 (2021) 114.
- [14] V.L. Solozhenko, S.F. Matar, Prediction of novel ultrahard phases in the B-C-N system from first principles: progress and problems, *Materials* 16 (2023) 886.
- [15] X.Y. Wang, Y.J. Wang, M. Zhang, H.Y. Liu, Superhard BC₂N in cubic diamondlike structure, *Phys. Rev. B* 107 (2023), 134101.
- [16] T.F. Xu, Z.R. Liu, D. Legut, R.F. Zhang, Anomalous bond softening mediated by strain-induced Friedel-like oscillations in a BC₂N superlattice, *Phys. Rev. B* 106 (2022), L060101.
- [17] Q. Gao, K. Luo, F.F. Ling, Q. Huang, L. Zhu, Q.Y. Han, Y. Zhang, Y.F. Gao, J.L. He, D.L. Yu, Theoretical study on the controllable preparation of superhard BC₂N under high pressure, *J. Mater. Chem. C* 10 (2022) 1660–1665.
- [18] S.Y. Chen, X.G. Gong, S.H. Wei, Superhard pseudocubic BC₂N superlattices, *Phys. Rev. Lett.* 98 (2007), 015502.
- [19] R.Q. Zhang, K.S. Chan, H.F. Cheung, S.T. Lee, Energetics of segregation in β -C₂BN, *Appl. Phys. Lett.* 75 (1999) 2259.
- [20] Y. Zhao, D.W. He, L.L. Daemen, T.D. Shen, R.B. Schwarz, Y. Zhu, D.L. Bish, J. Huang, J. Zhang, G. Shen, J. Qian, T.W. Zerda, Superhard B-C-N materials synthesized in nanostructured bulks, *J. Mater. Res.* 17 (2002) 3139–3145.
- [21] V.L. Solozhenko, D. Andrault, G. Fiquet, M. Mezouar, D.C. Rubie, Synthesis of superhard cubic BC₂N, *Appl. Phys. Lett.* 78 (2001) 1385–1387.
- [22] H. Sun, S.H. Jhi, D. Roundy, M.L. Cohen, S.G. Louie, Structural forms of cubic BC₂N, *Phys. Rev. B* 64 (2001), 094108.
- [23] X.F. Zhou, J. Sun, Y.X. Fan, J. Chen, H.T. Wang, X.J. Guo, J.L. He, Y.J. Tian, Most likely phase of superhard BC₂N by *ab initio* calculations, *Phys. Rev. B* 76 (2007), 100101.
- [24] X.G. Luo, X.J. Guo, B. Xu, Q.H. Wu, Q.K. Hu, Body-centered superhard BC₂N phases from first principles, *Phys. Rev. B* 76 (2007), 094103.
- [25] X.G. Luo, X.J. Guo, Z.Y. Liu, J.L. He, D.L. Yu, B. Xu, Y.J. Tian, First-principles study of wurtzite BC₂N, *Phys. Rev. B* 76 (2007), 092107.
- [26] Q. Li, M. Wang, A.R. Oganov, T. Cui, Y.M. Ma, G.T. Zou, Rhombohedral superhard structure of BC₂N, *J. Appl. Phys.* 105 (2009), 053514.
- [27] Y. Zhang, H. Sun, C.F. Chen, Superhard cubic BC₂N compared to diamond, *Phys. Rev. Lett.* 93 (2004), 195504.
- [28] Y. Zhang, H. Sun, C.F. Chen, Atomistic deformation modes in strong covalent solids, *Phys. Rev. Lett.* 94 (2005), 145505.
- [29] Z.C. Pan, H. Sun, C.F. Chen, Colossal shear-strength enhancement of low-density cubic BC₂N by nanoindentation, *Phys. Rev. Lett.* 98 (2007), 135505.
- [30] S.Y. Chen, X.G. Gong, S.H. Wei, Crystal structures and mechanical properties of superhard BC₂N and BC₄N alloys: first-principles calculations, *Phys. Rev. B* 77 (2008), 014113.
- [31] R. Ding, Y.J. Yao, B.H. Sun, G. Liu, J.G. He, T. Li, X.H. Wan, Z.B. Dai, D. Ponge, D. Raabe, C. Zhang, A. Godfrey, G. Miyamoto, T. Furuhara, Z.G. Yang, S.V. D. Zwaag, H. Chen, Chemical boundary engineering: a new route toward lean, ultrastrong yet ductile steels, *Sci. Adv.* 6 (2020) eaay1430.
- [32] S.Z. Chavoshi, P.S. Branicio, Q. An, Transition between Hall-Petch and inverse Hall-Petch behavior in nanocrystalline silicon carbide, *Phys. Rev. Mater.* 5 (2021), 073606.

- [33] Y.J. Tian, B. Xu, D.L. Yu, Y.M. Ma, Y.B. Wang, Y.B. Jiang, W.T. Hu, C.C. Tang, Y. F. Gao, K. Luo, Z.S. Zhao, L.M. Wang, B. Wen, J.L. He, Z.Y. Liu, Ultrahard nanotwinned cubic boron nitride, *Nature* 493 (2013) 385–388.
- [34] T.Y. Jin, M.D. Ma, B.Z. Li, Y.F. Gao, Q.L. Zhao, Z.S. Zhao, J.Y. Chen, Y.J. Tian, Mechanical polishing of ultrahard nanotwinned diamond via transition into hard sp^2-sp^3 amorphous carbon, *Carbon* 161 (2020) 1–6.
- [35] Y.L. Pan, P. Ying, Y.F. Gao, P. Liu, K. Tong, D.L. Yu, K.L. Jiang, W.T. Hu, B.Z. Li, B. Liu, Z.S. Zhao, J.L. He, B. Xu, Z.Y. Liu, Y.J. Tian, Extreme mechanical anisotropy in diamond with preferentially oriented nanotwin bundles, *Proc. Natl. Acad. Sci. USA* 118 (2021), e2108340118.
- [36] P.H. Li, Y.Q. Bu, L.Y. Wang, C. Wang, J.Q. Huang, K. Tong, Y.J. Chen, J.L. He, Z. S. Zhao, B. Xu, Z.Y. Liu, G.Y. Gao, A.M. Nie, H.T. Wang, Y.J. Tian, *In situ* observation of fracture along twin boundaries in boron carbide, *Adv. Mater.* (2022), 2204375, <https://doi.org/10.1002/adma.202204375>.
- [37] J.W. Xiao, H.Z. Yang, X.Z. Wu, F. Younus, P. Li, B. Wen, X.Y. Zhang, Y.B. Wang, Y. J. Tian, Dislocation behaviors in nanotwinned diamond, *Sci. Adv.* 4 (2018) eaat8195.
- [38] B. Li, H. Sun, C.F. Chen, Extreme mechanics of probing the ultimate strength of nanotwinned diamond, *Phys. Rev. Lett.* 117 (2016), 116103.
- [39] B. Li, H. Sun, C.F. Chen, Large indentation strain-stiffening in nanotwinned cubic boron nitride, *Nat. Commun.* 5 (2014) 4965.
- [40] W. Kohn, L.J. Sham, Self-consistent equations including exchange and correlation effects, *Phys. Rev.* 140 (1965) A1133.
- [41] J.P. Perdew, A. Zunger, Self-interaction correction to density-functional approximations for many-electron systems, *Phys. Rev. B* 23 (1981) 5048.
- [42] D.M. Ceperley, B.J. Alder, Ground state of the electron gas by a stochastic method, *Phys. Rev. Lett.* 45 (1980) 566.
- [43] G. Kresse, J. Furthmüller, Efficient iterative schemes for *ab initio* total-energy calculations using a plane-wave basis set, *Phys. Rev. B* 54 (1996) 11169.
- [44] P.E. Blöchl, Projector augmented-wave method, *Phys. Rev. B* 50 (1994) 17953.
- [45] H.J. Monkhorst, J.D. Pack, Special points for Brillouin-zone integrations, *Phys. Rev. B* 13 (1976) 5188.
- [46] A. Togo, F. Oba, I. Tanaka, First-principles calculations of the ferroelastic transition between rutile-type and CaCl_2 -type SiO_2 at high pressures, *Phys. Rev. B* 78 (2008), 134106.
- [47] A. Togo, F. Oba, I. Tanaka, Transition pathway of CO_2 crystals under high pressures, *Phys. Rev. B* 77 (2008), 184101.
- [48] R. Hill, The elastic behaviour of a crystalline aggregate, *Proc. Phys. Soc. Lond. Sect. A* 65 (1952) 349.
- [49] X.Q. Chen, H.Y. Niu, D.Z. Li, Y.Y. Li, Modeling hardness of polycrystalline materials and bulk metallic glasses, *Intermetallics* 19 (2011) 1275–1281.
- [50] Y.J. Tian, B. Xu, Z.S. Zhao, Microscopic theory of hardness and design of novel superhard crystals, *Int. J. Refract. Met. Hard Mater.* 33 (2012) 93–106.
- [51] D. Roundy, C.R. Krenn, M.L. Cohen, J.W. Morris Jr., Ideal shear strengths of fcc aluminum and copper, *Phys. Rev. Lett.* 82 (1999) 2713.
- [52] Z.C. Pan, H. Sun, Y. Zhang, C.F. Chen, Harder than diamond: superior indentation strength of wurtzite BN and lonsdaleite, *Phys. Rev. Lett.* 102 (2009), 055503.
- [53] W.G. Gong, C. Liu, X.Q. Song, Q. Li, Y.M. Ma, C.F. Chen, Unravelling the structure and strength of the highest boride of tungsten $\text{WB}_{4.2}$, *Phys. Rev. B* 100 (2019), 220102.
- [54] C. Liu, X.Q. Song, Q. Li, Y.M. Ma, C.F. Chen, Smooth flow in diamond: atomistic ductility and electronic conductivity, *Phys. Rev. Lett.* 123 (2019), 195504.
- [55] C. Liu, X.Q. Song, Q. Li, Y.M. Ma, C.F. Chen, Superconductivity in compression-shear deformed diamond, *Phys. Rev. Lett.* 124 (2020), 147001.
- [56] C. Liu, X.Q. Song, Q. Li, Y.M. Ma, C.F. Chen, Superconductivity in shear strained semiconductors, *Chin. Phys. Lett.* 38 (2021), 086301.
- [57] X.Q. Song, C. Liu, Q. Li, R.J. Hemley, Y.M. Ma, C.F. Chen, Stress-induced high- T_c superconductivity in solid molecular hydrogen, *Proc. Natl. Acad. Sci. USA* 119 (2022), e2122691119.
- [58] See Supplemental Material for the twin-structure information of BC_2N , the phonon spectra of $\beta\text{-BC}_2\text{N}$ and $\tau\text{-BC}_2\text{N}$, the pure and Vickers shear stress-strain relations of $\beta\text{-BC}_2\text{N}$ (2023).
- [59] E.O. Hall, The deformation and ageing of mild steel: III discussion of results, *Proc. Phys. Soc. B* 64 (1951) 747.
- [60] N.J. Petch, The cleavage strength of polycrystals, *J. Iron Steel Res. Int.* 174 (1953) 25–28.
- [61] J.S. Tse, D.D. Klug, F.M. Gao, Hardness of nanocrystalline diamonds, *Phys. Rev. B* 73 (2006), 140102.
- [62] J.C. Phillips, Ionicity of the chemical bond in crystals, *Rev. Mod. Phys.* 42 (1970) 317–356.
- [63] B. Yang, X.H. Peng, C. Huang, Z.C. Wang, D.Q. Yin, T. Fu, Strengthening and toughening by partial slip in nanotwinned diamond, *Carbon* 150 (2019) 1–7.
- [64] Z.J. Han, H. Liu, Q. Li, D. Zhou, J. Lv, Superior mechanical properties of GaAs driven by lattice nanotwinning, *Chin. Phys. Lett.* 38 (2021), 046201.
- [65] G.D. Li, S.I. Morozov, Q.J. Zhang, Q. An, P.C. Zhai, G.J. Snyder, Enhanced strength through nanotwinning in the thermoelectric semiconductor InSb, *Phys. Rev. Lett.* 119 (2017), 215503.
- [66] B. Wen, B. Xu, Y.B. Wang, G.Y. Gao, X.F. Zhou, Z.S. Zhao, Y.J. Tian, Continuous strengthening in nanotwinned diamond, *npj Comput. Mater.* 5 (2019) 117.
- [67] J.W. Xiao, B. Wen, B. Xu, X.Y. Zhang, Y.B. Wang, Y.J. Tian, Intersectional nanotwinned diamond—the hardest polycrystalline diamond by design, *npj Comput. Mater.* 6 (2020) 119.

Supplemental Material for
Theoretical Design of Superhard Twinned BC₂N

Nan Min,^{a,b} Hui Liang,^a Hao Chen,^c Xianqi Song,^{a,*} Dan Zhou,^{c,*} and Quan Li^{a,b,*}

^a*State Key Lab of Superhard Materials and Key Laboratory of Material Simulation Methods & Software of Ministry of Education, College of Physics, Jilin University, Changchun 130012, China*

^b*International Center of Future Science, Jilin University, Changchun 130012, China*

^c*School of Physics, Changchun University of Science and Technology, Changchun 130022, China*

*Corresponding author.

Email address:

sxq@calypso.cn (X.Q. Song); zhoudan@cust.edu.cn (D. Zhou); liquan777@jlu.edu.cn (Q. Li)

Here we provide supplemental details on the twin-structure information of BC₂N (Tables S1 and S2), phonon spectra of β -BC₂N and τ -BC₂N (Fig. S1), pure and Vickers shear stress-strain relations of β -BC₂N (Fig. S2), key bond length variation and structural snapshots of twinned BC₂N under Vickers indentation (Fig. S3).

Table S1. The structural information of twin-BC₂N.

Twinned Structure	Space group	Lattice parameter (Å, °)				Number of atoms	Volume (Å ³ /f.u.)
		<i>a</i>	<i>b</i>	<i>c</i>	α, β, γ		
BC ₂ N-1	<i>Pmn2</i> ₁	2.508	4.393	12.426		24	22.81
BC ₂ N-2	<i>Cc</i>	5.057	8.706	13.417	$\beta = 111.9$	96	22.84
BC ₂ N-3	<i>Pmc2</i> ₁	2.504	4.393	12.477		24	22.88
BC ₂ N-4	<i>Pmn2</i> ₁	2.512	4.401	12.439		24	22.92
BC ₂ N-5	<i>C2</i>	5.066	8.722	13.443	$\beta = 111.9$	96	22.95
BC ₂ N-6	<i>Pmm2</i>	2.508	4.400	12.503		24	23.00
BC ₂ N-7	<i>Pm</i>	2.518	4.386	12.428	$\alpha = 90.2$ $\alpha = 90.4$	24	22.88
BC ₂ N-8	<i>P1</i>	5.035	5.059	12.432	$\beta = 89.7$ $\gamma = 119.9$	48	22.88
BC ₂ N-9	<i>Pm</i>	2.515	4.391	12.430	$\alpha = 90.2$	24	22.88
BC ₂ N-10	<i>Pm</i>	2.521	4.395	12.462	$\alpha = 90.3$ $\alpha = 90.4$	24	23.02
BC ₂ N-11	<i>P1</i>	5.043	5.067	12.454	$\beta = 89.7$ $\gamma = 119.8$	48	23.00
BC ₂ N-12	<i>Pm</i>	2.521	4.395	12.439	$\alpha = 90.3$	24	22.97
BC ₂ N-13	<i>Pmc2</i> ₁	2.525	4.382	12.403		24	22.88
BC ₂ N-14	<i>Cc</i>	5.060	8.762	13.357	$\beta = 111.7$	96	22.93
BC ₂ N-15	<i>Pmn2</i> ₁	2.532	4.384	12.418		24	22.97
BC ₂ N-16	<i>Pmn2</i> ₁	2.531	4.386	12.433		24	23.00
BC ₂ N-17	<i>C2</i>	5.068	8.776	13.484	$\beta = 112.7$	96	23.05
BC ₂ N-18	<i>Pmm2</i>	2.537	4.389	12.444		24	23.09

Table S2. The structural information of τ -BC₂N.

Twin Structure	Lattice constants (\AA)	Atom	Position (x, y, z)		
			x	y	z
τ -BC ₂ N	$a=2.508$ $b=4.393$ $c=12.426$	B (2a)	0.500	0.254	-0.877
		B (2a)	-0.500	-0.088	-0.544
		B (2a)	-0.500	0.582	-0.708
		C (2a)	-0.000	0.082	-0.709
		C (2a)	-1.000	-0.252	-0.874
		C (2a)	-1.000	0.411	-0.541
		C (2a)	0.500	0.251	-0.498
		C (2a)	-0.500	-0.074	-0.670
		C (2a)	-0.500	0.590	-0.834
		N (2a)	0.000	-0.262	-0.503
		N (2a)	0.000	0.410	-0.664
		N (2a)	0.000	0.083	-0.833

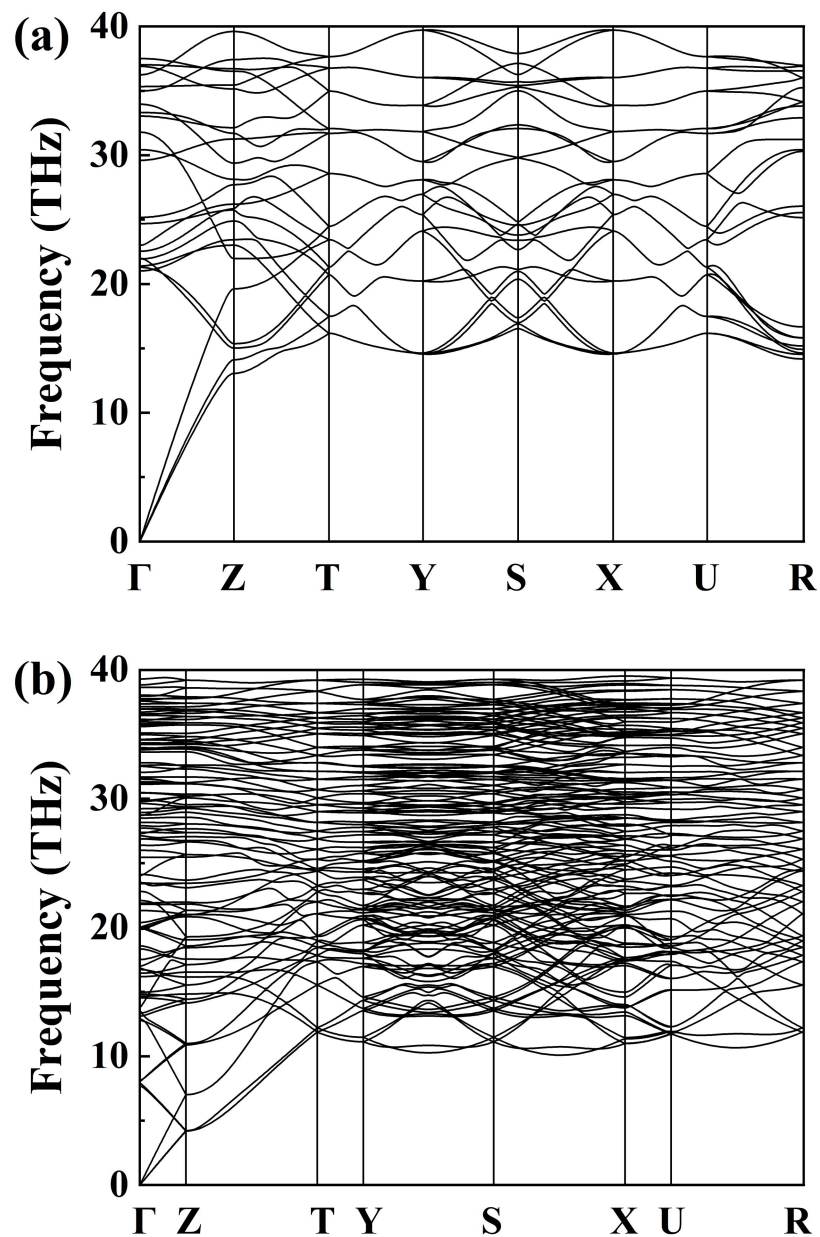


Fig. S1. The theoretical phonon spectra of (a) β - BC_2N and (b) τ - BC_2N .

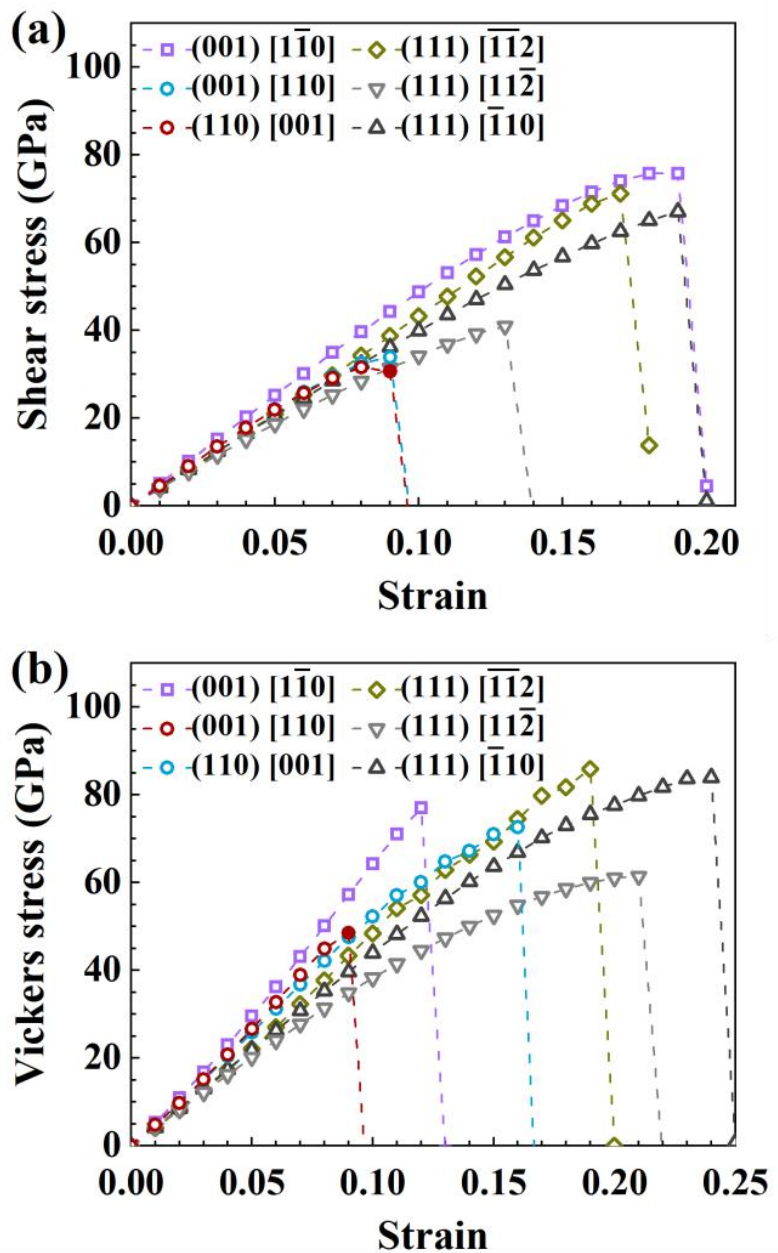


Fig S2. Calculated stress-strain relations of β - BC_2N under pure shear (a) and Vickers shear (b) along various directions.

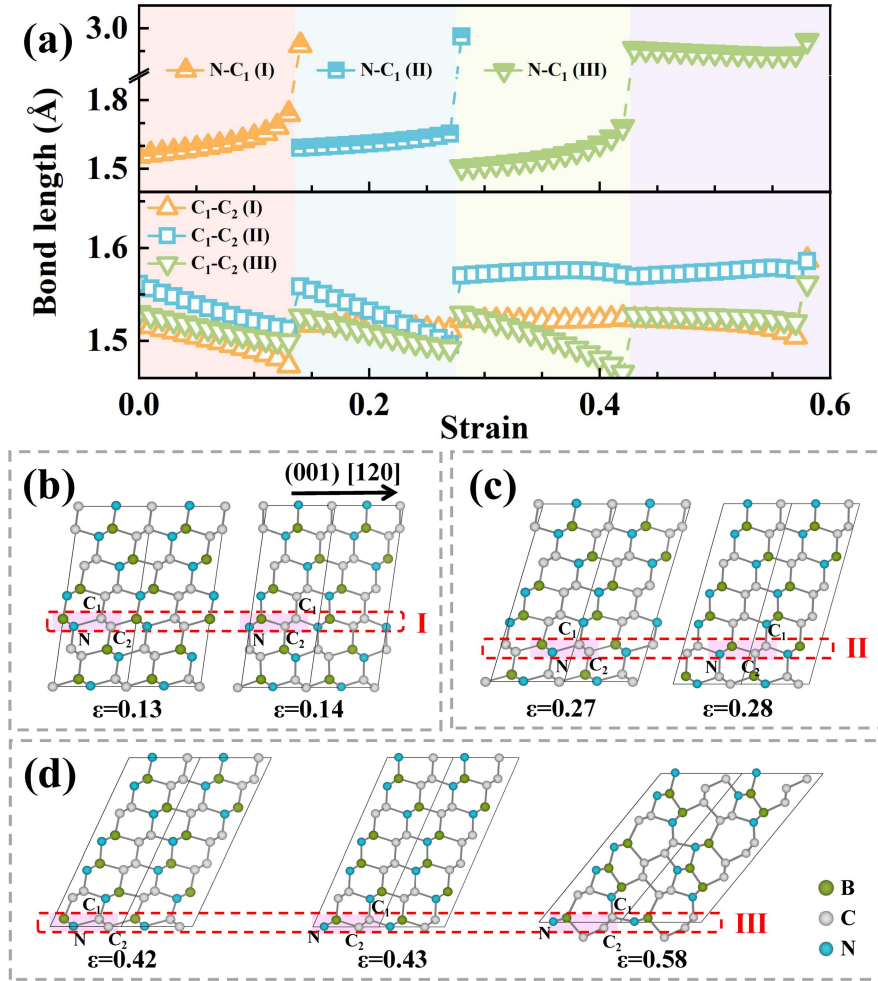


Fig. S3. (a) Key bond length variation in twinned BC₂N with increasing shear strain along (001)[120] direction under Vickers indentation. (b)–(d) Structural snapshots of twinned BC₂N in three bond-rearrangement processes: layer I at the strain of 0.13, layer II at 0.27, and layer III at 0.42. We further considered more complex loading conditions, such as the biaxial stress field, which combines normal compression and transverse shear deformation, to assess the stress responses of twinned BC₂N under Vickers indentation. The evolution of key bond lengths with increasing strain and critical structural snapshots along the (001)[120] Vickers shear direction is presented in Fig. S3. The Vickers shear strength of τ -BC₂N can reach 100.0 GPa at a strain of 0.57, surpassing the Vickers shear strength of monocrystalline diamond. Both the deformation process and strengthening mechanism mirror those under pure shear conditions, demonstrating the robustness of the fascinating TB-mediated strengthening phenomena in BC₂N.